larger size of CdTe or may possibly reflect lattice distortion in incorporating Cr^+ for Zn.

The variation in the interaction of Cr^+ with second-neighbor sites as compared to the lack of variation for Mn^{++} is undoubtedly due to the greater extent of the Cr^+ wave function as compared to Mn^{++}. This is to be expected since Cr in this configuration has accepted an electron. Mn^{++}, on the other hand, is electrically neutral.

In summary, the resonance measurements that have been made of Cr^+ in four zinc-blende lattices show that there are variations from crystal to crystal of the resonance parameters g, a, $A(Cr^{53})$, and $A_{Zn,Cd}$. The variations are consistent with changes in the degree of covalency in the bonds and with lattice distortions caused by incorporating the larger Cr^+ in place of divalent zinc.

ACKNOWLEDGMENTS

I wish to thank Dr. L. Suchow, J. Scardefield, and J. Kucza who grew the crystals and E. E. Tynan for aid in taking the paramagnetic data.

PHYSICAL REVIEW VOLUME 133, NUMBER 6A 16 MARCH 1964

Longitudinal Nuclear Spin-Spin Relaxation*

R. L. STROMBOTNE† AND E. L. HAHN
Department of Physics, University of California, Berkeley, California
(Received 25 October 1963)

A theoretical and experimental study is made of the nuclear magnetization which appears after a sudden unidirectional step magnetic field is applied nonadiabatically to an ordered spin system which has been prepared by the process of adiabatic demagnetization. The magnetization exhibits damped oscillations about a nonvanishing equilibrium value. The oscillation frequencies correspond to the fundamental and harmonic components of Larmor frequency determined by the combined effect of local dipole and external step fields. The oscillations arise as the internally ordered dipole-dipole interaction energy exchanges with the suddenly imposed Zeeman energy reservoir. A density matrix calculation carried to second order in time-dependent perturbation theory, combined with a Gaussian decay model, accounts for the observed oscillations within times comparable to the decay time. Fluorine nuclei in single CaF_2 crystals are studied for various crystal orientations with respect to the applied step field. For long times after step field application the attainment of thermal equilibrium between dipole-dipole and Zeeman reservoirs permits prediction, using the spin temperature concept, of magnetization developed along the step field.

I. INTRODUCTION

FOLLOWING the sudden reorientation of equilibrium nuclear magnetization M_0 by a radio-frequency (rf) pulse, a transient nuclear induction signal appears which is a measure of the Fourier integral of the resonance line shape.[1,2] The relaxation time of this signal, loosely referred to as T_2, is a measure of the lifetime of coherent magnetization which precesses in the transverse direction perpendicular to a large polarizing magnetic field H_0. In this paper the transient response of the spin system is studied after a step direct current (dc) magnetic field H_s is applied to an ordered spin system in zero ($H_0=0$) magnetic field.[3] The ordered spin state is prepared by carrying out an adiabatic demagnetization of the initially polarized sample by turning off H_0 slowly.[4] The step field H_s is then turned on nonadiabatically in a time much shorter than the Larmor period of the spins in the net field determined by H_s and the mean local dipolar field H_L. A longitudinal nuclear magnetization $\langle M_z(t)\rangle$ develops in time along the direction of H_s after it is applied. A transient longitudinal spin-spin relaxation (LSSR) behavior is displayed by $\langle M_z(t)\rangle$, which is a measure of the oscillatory interchange of energy between the magnetic dipole-dipole energy reservoir and the suddenly imposed Zeeman energy reservoir. In a sense, these measurements yield the Fourier integral of line-shape measurements made by Anderson[5] on the nuclear magnetic absorption of spins ordered in low magnetic fields comparable to H_L. The transient measurements reveal directly the time evolution toward internal spin-spin equilibrium and toward final thermal equilibrium between Zeeman and dipole-dipole energy reservoirs.

A number of observers[4,6,7] have investigated various

* Supported by the National Science Foundation and the U. S. Office of Naval Research.

† Submitted in partial fulfullment of the degree of Doctor of Philosophy. Present address: National Bureau of Standards, Boulder, Colorado.

[1] E. L. Hahn, Phys. Rev. **80**, 580 (1950).

[2] I. Lowe and R. E. Norberg, Phys. Rev. **107**, 46 (1957); B. Herzog and E. L. Hahn, *ibid.* **103**, 148 (1956).

[3] R. L. Strombotne and E. L. Hahn, Bull. Am. Phys. Soc. **6**, 508 (1961).

[4] A. Abragam and W. G. Proctor, Phys. Rev. **109**, 1441 (1958).

[5] A. G. Anderson, Phys. Rev. **125**, 1517 (1962); **115**, 863 (1959).

[6] S. R. Hartmann and A. G. Anderson, Phys. Rev. **128**, 2023 (1962); S. R. Hartmann and E. L. Hahn, *ibid.* **128**, 2042 (1962); F. M. Lurie and C. P. Slichter, Phys. Rev. Letters **10**, 403 (1963).

[7] R. T. Schumacher, Phys. Rev. **112**, 837 (1958); P. S. Pershan,

aspects of nuclear relaxation in which nonoscillatory changes in spin populations occur, relating more directly to systems which can be assigned one or more spin temperatures. In the present investigation of the F^{19} nuclear magnetization in CaF_2 single crystals, one may only use the spin temperature concept after the transient oscillations of $\langle M_z(t)\rangle$ have disappeared and the dipole-dipole and Zeeman reservoirs have attained internal equilibrium. The very long spin-lattice relaxation times are to be neglected in considering the theoretical and experimental results. Waller[8] was the first to consider theoretically the process of LSSR in an electron paramagnetic system. He found in the special case $H_s \ll H_L$ that a thermal equilibrium magnetization $\langle M_z\rangle \approx CH_s/T$ finally appears, where T is the initial temperature of the spin system in zero external field and C is the Curie constant. The Zeeman energy $W=-\langle M_z\rangle H_s$ appears at the expense of internal dipole-dipole energy which resides in the system prior to the application of the step field. Waller also found that the magnetization appears as a sum of oscillating terms which represent the eigenfrequencies of the system directly after H_s is suddenly applied. We extend Waller's treatment here to include a greater range in values of step field H_s and consider the nuclear dipole-dipole interaction to be the sole contributor to the zero field energy. No type of scalar spin-spin exchange energy is included.

Figure 1 shows schematically the sequence of magnetic fields applied to the spin sample in our experiments. Following adiabatic demagnetization from a field $H_0 \gg H_L$, a step field H_s, usually comparable to H_L, is applied at time $t=0$, after which time the spin system evolves in the field H_s. A second step field H_B greater than H_L and H_s is then applied at $t=t_B$, and the evolution of magnetization $\langle M_z\rangle$ in the field H_s is interrupted. One could, in principle, measure the magnetization which develops at the time t_B by a pulsed nuclear resonance measurement directly in the field H_s, but the signals are too weak to make useful measurements. It is necessary therefore to apply a second step field H_B at $t=t_B$, and the particular magnetization which the spin system has at that time is retained and finally displayed after an adiabatic remagnetization back into the high field H_0. A nuclear signal in the field H_0 can then be obtained by pulsed resonance or by adiabatic fast passage, which is a measurement linearly dependent upon $\langle M_z(t)\rangle$ at $t=t_B$. The entire sequence of field switching must take place in a time short compared to the spin-lattice relaxation time. By repeating the sequence for various values of t_B for given H_s and H_B, the transient response of the spin system can be determined. The field dependence of the equilibrium magnetization which develops after a long time can also be obtained by varying H_s while keeping H_B constant.

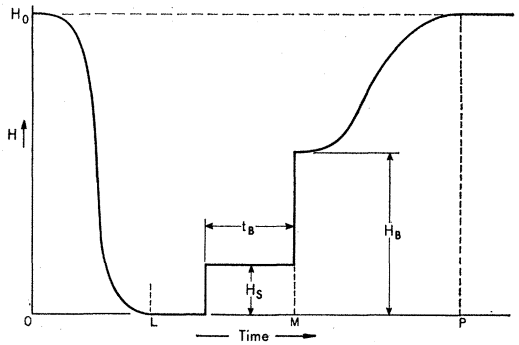

FIG. 1. Magnetic field applied to the nuclear spin sample as a function of time. In time regions $O \rightarrow L$ and $M \rightarrow P$, adiabatic demagnetization and remagnetization occur, respectively. At P, a 90° pulse inspection is made of the magnetization.

II. THERMAL EQUILIBRIUM THEORY OF LSSR

After the step field H_s has been applied, the equilibrium Zeeman energy and magnetization can be rigorously determined if t_B is sufficiently long so that the two heat reservoirs characterized by the Zeeman energy $\langle \mathcal{H}_0\rangle$ and the dipole-dipole energy $\langle \mathcal{H}_{dd}\rangle$ will arrive at a common temperature. The Hamiltonian of the system is

$$\mathcal{H}=\mathcal{H}_0+\mathcal{H}_{dd}, \tag{1}$$

where

$$\mathcal{H}_0=-\hbar H\sum_{i=1}^{N}\gamma_i I_{zi} \tag{2}$$

is the interaction energy of N spins in the rigid lattice with the external field H, γ is the gyromagnetic ratio, and I is the spin operator. The dipole-dipole interaction $\mathcal{H}_{dd}$ will be given explicitly in Sec. III.

The reader is referred to the paper of Abragam and Proctor[4] for the origins of expressions based upon the density matrix method which will be used to analyze the thermal equilibrium of spin ensembles in our experiments. At a spin temperature T, the ensemble has the density matrix

$$\rho=\frac{\exp(-\mathcal{H}/kT)}{\mathrm{Tr}\{\exp(-\mathcal{H}/kT)\}}. \tag{3}$$

In the high-temperature approximation

$$\langle \mathcal{H}_{dd}\rangle=\frac{-\mathrm{Tr}\{\mathcal{H}_{dd}^2\}}{kT\ \mathrm{Tr}1}; \tag{4}$$

obtained from the relation $\langle \mathcal{H}_{dd}\rangle=\mathrm{Tr}\{\mathcal{H}_{dd}\rho\}$. Henceforth all traces will be taken as normalized so that Tr1 will be replaced by unity. The local field H_L is defined from

$$H_L^2=-\mathrm{Tr}\{\mathcal{H}_{dd}^2\}/\mathrm{Tr}\{M_z^2\}, \tag{5}$$

where the operator M_z is given by

$$M_z=\hbar\sum_{i=1}^{N}\gamma_i I_{zi}. \tag{6}$$

---

ibid. **117**, 109 (1960); A. Landesman and M. Goldman, Compt. Rend. **252**, 263 (1961).

[8] I. Waller, Z. Physik **79**, 370 (1932).

The thermal equilibrium magnetization in constant field H is

$$\langle M_z\rangle = CH/T, \tag{7}$$

where

$$C=\frac{\mathrm{Tr}\{M_z^2\}}{k}=\frac{I(I+1)N\hbar^2\gamma^2}{3k}, \tag{8}$$

and the Zeeman energy is given by

$$\langle \mathcal{H}_0\rangle = -(CH^2/T). \tag{9}$$

Following adiabatic demagnetization by reducing H_0 to zero, according to Fig. 1, the final spin temperature $T_i=T_0H_L/H_0$ is reached,[4] where T_0 is the laboratory lattice temperature. The resulting zero-field dipole-dipole energy

$$\langle \mathcal{H}_{dd}(i)\rangle = -CH_L^2/T_i \tag{10}$$

will divide between the equilibrium dipole-dipole and Zeeman energies $\langle \mathcal{H}_{dd}(s)\rangle$ and $\langle \mathcal{H}_0(s)\rangle$, respectively, after the application of step field H_s, so that

$$\langle \mathcal{H}_{dd}(i)\rangle = \langle \mathcal{H}_{dd}(s)\rangle + \langle \mathcal{H}_0(s)\rangle = -\frac{C(H_s^2+H_L^2)}{T_s}. \tag{11}$$

From Eqs. (10) and (11) the final spin temperature T_s is obtained as

$$\frac{1}{T_s}=\left(\frac{1}{T_i}\right)\left(\frac{H_L^2}{H_s^2+H_L^2}\right). \tag{12}$$

Substitution of $1/T_s$ into Eqs. (7), (9), and (10) gives

$$\langle \mathcal{H}_0(s)\rangle = -\left(\frac{CH_L^2}{T_i}\right)\left(\frac{H_s^2}{H_s^2+H_L^2}\right), \tag{13}$$

$$\langle \mathcal{H}_{dd}(s)\rangle = -\left(\frac{CH_L^2}{T_i}\right)\left(\frac{H_L^2}{H_s^2+H_L^2}\right), \tag{14}$$

and

$$\langle M_z(s)\rangle = \left(\frac{CH_L}{T_i}\right)\left(\frac{H_sH_L}{H_s^2+H_L^2}\right). \tag{15}$$

The effect of the second step field H_B is essential to the actual recording of $\langle M_z\rangle$ data, and will require again the same considerations of energy conservation as given above. Let H_B be applied in the same direction as H_s at a time t_B after H_s is turned on. The dipole-dipole energy $\langle \mathcal{H}_{dd}(t_B)\rangle$ at any arbitrary time t_B and the corresponding magnetization $\langle M_z(t_B)\rangle$ exist whether or not spin-spin thermal equilibrium is achieved. The sudden appearance of H_B has no immediate effect upon the dipole-dipole energy, but the Zeeman energy is abruptly switched from $-\langle M_z(t_B)\rangle H_s$ to $-\langle M_z(t_B)\rangle H_B$ at time t_B. Just before H_B is turned on, the total energy of the system is

$$\langle \mathcal{H}_{dd}(i)\rangle - \langle \mathcal{H}_{dd}(t_B)\rangle = \langle M_z(t_B)\rangle H_s, \tag{16}$$

and immediately after H_B is switched on, the total energy is

$$\begin{aligned}\langle \mathcal{H}(t_B)\rangle &= \langle \mathcal{H}_{dd}(t_B)\rangle - \langle M_z(t_B)\rangle H_B \\ &= \langle \mathcal{H}_{dd}(i)\rangle - (H_B-H_s)\langle M_z(t_B)\rangle.\end{aligned} \tag{17}$$

An equilibrium spin temperature T_B will now result after a long time and the energy becomes

$$\langle \mathcal{H}(B)\rangle = -C((H_B^2+H_L^2)/T_B). \tag{18}$$

After combining Eqs. (17) and (18), one obtains

$$\frac{1}{T_B}=\frac{-\langle \mathcal{H}_{dd}(i)\rangle + (H_B-H_s)\langle M_z(t_B)\rangle}{C(H_B^2+H_L^2)}. \tag{19}$$

The equilibrium magnetization developed in H_B is, therefore,

$$\langle M_z(B)\rangle = \frac{H_B(H_B-H_s)}{H_B^2+H_L^2}\langle M_z(t_B)\rangle + \left(\frac{CH_L}{T_i}\right)\left(\frac{H_LH_B}{H_B^2+H_L^2}\right). \tag{20}$$

It is important to note that the first term in Eq. (20) is proportional to the magnetization $\langle M_z(t_B)\rangle$ developed after the first step field H_s is applied. This $\langle M_z(t_B)\rangle$ term, although it may be a transient value, contributes to the equilibrium value of $\langle M_z(B)\rangle$ after the second step field H_B is applied. It is preferable to keep $H_B>H_s$ with both fields constant in amplitude. Then $\langle M_z(B)\rangle$ is a measure of the transient response of the system to a single step field H_s, since $\langle M_z(B)\rangle$ is a linear function of $\langle M_z(t_B)\rangle$ and may vary as t_B is changed. A signal proportional to $\langle M_z(B)\rangle$ is measured finally in terms of a free precession signal after adiabatic remagnetization to a high magnetic field H_0.

From Eq. (20), let the incremental change in $\langle M_z(B)\rangle$ be defined as

$$\Delta\langle M_z\rangle = \frac{H_B(H_B-H_s)\langle M_z(t_B)\rangle}{H_B^2+H_L^2}. \tag{21}$$

If $\langle M_z(t_B)\rangle$ is the equilibrium magnetization as given by Eq. (15), then the corresponding incremental magnetization is

$$\Delta\langle M_z\rangle_{\mathrm{eq}} = \left(\frac{CH_L}{T_i}\right)\left(\frac{H_B[H_B-H_s]}{H_B^2+H_L^2}\right)\left(\frac{H_sH_L}{H_s^2+H_L^2}\right), \tag{21a}$$

which has a maximum value when $H_s\approx H_L$, assuming that $H_B\gg H_L$. This provides a novel method for measuring H_L, as shown in Fig. 2, for F nuclei in CaF_2 single crystal, where H_s is applied in the $\langle 111\rangle$ direction.

III. THEORY OF TRANSIENT LSSR

We now inquire into the nature of the observed oscillations of $\langle M_z(t_B)\rangle$ directly following the application of step field H_s. For simplicity, assume that the local field

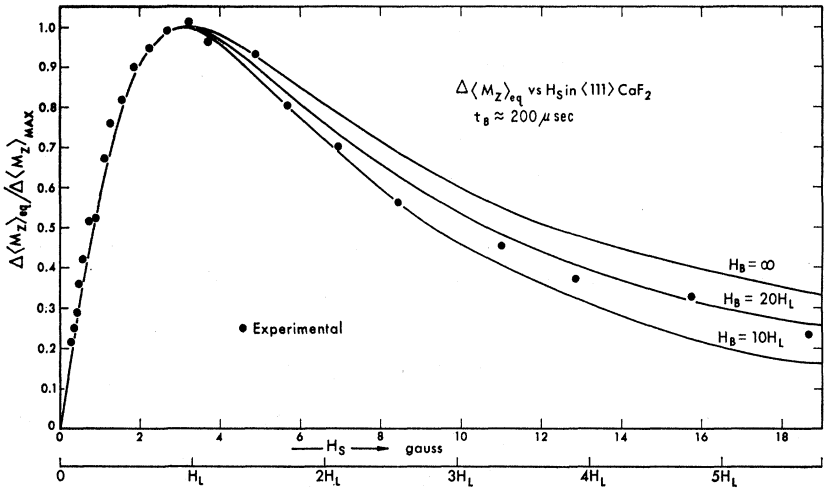

FIG. 2. Equilibrium fluorine nuclear magnetization as a function of applied step field H_s. The step field H_s is applied after adiabatic demagnetization of F nuclei in CaF_2 from high-field H_0.

remains static, as shown in Fig. 3, and that the resultant field at the site of an ordered i spin is given by $\mathbf{H}_i=\mathbf{H}_s+\mathbf{H}_L$ immediately after the application of H_s. The i spins begin to precess in phase at approximately the frequency $\omega_i=\gamma H_i$, and after a time comparable to $1/\gamma H_L$ the phases become random. The direction of H_s defines the z direction and the oscillating component of $\langle M_z\rangle$ will derive from those spins which do not lie parallel or antiparallel to H_s at the time of its application. In the limits of $H_s \gg H_L$ and $H_s \ll H_L$, this simple model shows a change in $\langle M_z\rangle$ which is proportional to $1/H_s$ and H_s, respectively, in agreement with Eq. (15) which refers to thermal equilibrium. Actually, the internal field H_L is itself not static, and because H_L will oscillate, it is found that second and higher harmonics of oscillation will appear in addition to the fundamental frequency γH_i displayed by $\langle M_z\rangle$.

A time-dependent perturbation method will now be applied to determine the transient response of $\Delta\langle M_z(t_B)\rangle$ to second order, valid in the limit that $H_s > H_L$ for the short time $t_B < 1/\gamma H_L$. The evolution toward thermal equilibrium for time $t_B \gg 1/\gamma H_L$, when the oscillations of $M_z(t_B)$ have died out, will not be discussed in detail in this paper. Analysis of the equilibration time constant to give final thermal equilibrium in this latter case has been given in detail by Caspers.[9] Others[10,11] have also applied the transient spin temperature approach to this and related phenomena.

From Eq. (16), the expression

$$\langle M_z(t_B)\rangle = \frac{\langle \mathcal{H}_{dd}(t_B)\rangle - \langle \mathcal{H}_{dd}(i)\rangle}{H_s} \tag{22}$$

indicates that a theory which evaluates $\langle \mathcal{H}_{dd}(t)\rangle$ (hereafter let $t_B=t$) will be tested by measurements of $\langle M_z(t)\rangle$. From an expansion of Eq. (3), the effective initial density matrix in zero field is given by

$$\rho_0 = -\mathcal{H}_{dd}/kT, \tag{23}$$

where we recall that the expression Tr1 is normalized to unity. After H_s is applied, the density matrix evolves as

$$\rho(t) = \exp(-i\mathcal{H}t)\rho_0 \exp(+i\mathcal{H}t), \tag{24}$$

where $\mathcal{H}$ is given by Eq. (1); $\hbar$ is chosen to be unity here and in all the analysis which follows. The explicit solution of

$$\langle \mathcal{H}_{dd}(t)\rangle = \mathrm{Tr}\{\mathcal{H}_{dd}\rho(t)\}$$

$$\approx -\frac{1}{kT}\mathrm{Tr}\{\mathcal{H}_{dd}\exp(-i\mathcal{H}t)\mathcal{H}_{dd}\exp(+i\mathcal{H}t)\} \tag{25}$$

is carried out to second order. Note that $\langle \mathcal{H}_{dd}(t)\rangle = \langle \mathcal{H}_{dd}(-t)\rangle$. It is convenient to express the equation[11]

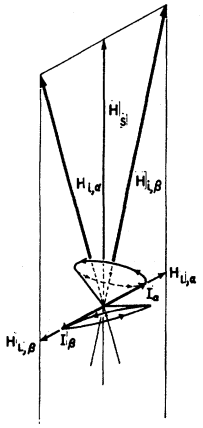

FIG. 3. Schematic representation of precession of ordered spins α and β following application of step field $\mathbf{H}_s$ to an adiabatically demagnetized sample. The local fields $\mathbf{H}_{L,\alpha}$ and $\mathbf{H}_{L,\beta}$ exist at α and β spin sites, respectively. After sudden application of $\mathbf{H}_s$, spins α and β precess about the respective resultant fields $\mathbf{H}_{i,\alpha}$ and $\mathbf{H}_{i,\beta}$.

[9] W. J. Caspers, Physica **26**, 778 (1960).
[10] S. R. Hartmann and A. G. Anderson, *Magnetic and Electric Resonance and Relaxation, Proceeding of Colloque Ampère, Eindhoven, July 1962*, edited by J. Schmidt (Interscience Publishers, Inc., New York, 1963), p. 157.
[11] A. Abragam, *Principles of Nuclear Magnetism* (Oxford University Press, New York, 1961).

for the density matrix as

$$i\frac{d\rho^*(t)}{dt}=[\mathcal{H}_{dd}^*(-t),\rho^*(t)], \tag{26}$$

where

$$\mathcal{H}_{dd}^*(-t)=T\mathcal{H}T^{-1}-\mathcal{H}_0=T\mathcal{H}_{dd}T^{-1},$$
$$\rho^*=T\rho(t)T^{-1},$$

and $T=\exp(+i\mathcal{H}_0t)$. With the formal solution of $\rho^*(t)$ expressed as a perturbation series

$$\rho^*(t)=\rho_0^*(0)+\rho_1^*(t)+\rho_2^*(t)+\cdots+\rho_n^*(t)+\rho_{n+1}^*\cdots, \tag{27}$$

the successive terms are related by

$$\rho_{n+1}^*(t)=-i\int_0^t dt'[\mathcal{H}_{dd}^*(-t'),\rho_n^*(t')], \tag{28}$$

and $\rho_0^*=\rho_0$ at $t=0$. In terms of $\rho^*(t)$, Eq. (25) now reads

$$\langle\mathcal{H}_{dd}(t)\rangle=\mathrm{Tr}\{\mathcal{H}_{dd}^*(-t)\rho^*(t)\}. \tag{29}$$

It will be useful at this point to write

$$\mathcal{H}_{dd}=\sum_{M=-2}^{+2}G_M, \tag{30}$$

where

$$G_M=\tfrac{1}{2}\sum_{k\neq l}U_{2M}^*(r_{kl})V_{2M}(J^k,J^l). \tag{30a}$$

The quantities U_{2M} and V_{2M} are the components of irreducible second-rank tensors on a spherical coordinate basis, referring to space and spin coordinates, respectively. Upon defining $\mathbf{r}_{kl}$ as the vector distance between spin l and spin k, $\Gamma_{kl}=\gamma_k\gamma_l r_{kl}^{-3}$, and ξ_{kl}, η_{kl}, ζ_{kl} as the direction cosines of r_{kl} with respect to the x, y, and z axes, respectively, the space components are:

$$U_{20}(r_{kl})=-\tfrac{1}{4}(\sqrt{6})\Gamma_{kl}(3\zeta_{kl}^2-1), \tag{31a}$$
$$U_{2\pm1}(r_{kl})=\pm\tfrac{3}{2}\Gamma_{kl}(\xi_k\pm i\eta_{kl})\zeta_{kl}, \tag{31b}$$
$$U_{2\pm2}(r_{kl})=-\tfrac{3}{4}\Gamma_{kl}(\xi_{kl}\pm i\eta_{kl})^2. \tag{31c}$$

The spin tensor components are

$$V_{20}(J^k,J^l)=\tfrac{2}{3}(\sqrt{6})[J_z{}^kJ_z{}^l+\tfrac{1}{2}(J_{+1}{}^kJ_{-1}{}^l+J_{-1}{}^kJ_{+1}{}^l)], \tag{32a}$$
$$V_{2\pm1}(J^k,J^l)=\sqrt{2}[J_{\pm1}{}^kJ_z{}^l+J_z{}^kJ_{\pm1}{}^l], \tag{32b}$$
$$V_{2\pm2}(J^k,J^l)=2J_{\pm1}{}^kJ_{\pm1}{}^l, \tag{32c}$$

where $J_{\pm1}{}^k=(1/\sqrt{2})(I_x{}^k\pm iI_y{}^k)$, $J_z{}^k=I_z{}^k=J_0{}^k$, and $\mathbf{I}$ is the spin operator. The useful commutation relations are

$$(J_z,J_m)=mJ_m \quad \text{for} \quad m=1,0,-1, \tag{33a}$$
$$(J_{+1},J_{-1})=J_z, \tag{33b}$$

and

$$(J_z,G_M)=MG_M, \tag{33c}$$

where $J_{z,\pm1}=\sum_k J_{z,\pm1}{}^k$. The useful transformation property

$$\exp(i\mathcal{H}_0t)G_M\exp(-i\mathcal{H}_0t)=G_M\exp(-iM\gamma Ht), \tag{34}$$

follows with the aid of Eqs. (2) and (33c), and $\gamma_k=\gamma_l=\gamma$.

In zero order, Eq. (29) gives

$$\langle\mathcal{H}_{dd}(t)\rangle_0=\mathrm{Tr}\{\mathcal{H}_{dd}^*(-t)\rho_0\}. \tag{35}$$

Combining Eqs. (23), (26), (30), and (34) with (35),

$$\langle\mathcal{H}_{dd}(t)\rangle_0=-\frac{1}{kT}\mathrm{Tr}\sum_{M=-2}^{2}\{G_M\sum_{M'=-2}^{2}G_{M'}\exp(iM'\omega_0t)\}, \tag{36}$$

where $\omega_0=\gamma H_s$. With the property that $\mathrm{Tr}\{G_MG_{-M'}\}=\delta_{M,M'}\mathrm{Tr}\{G_MG_{-M}\}$,

$$\langle\mathcal{H}_{dd}(t)\rangle_0=-\frac{1}{kT}\sum_{M=-2}^{2}\mathrm{Tr}\{G_MG_{-M}\}\cos M\omega_0t. \tag{37}$$

The five terms of $\langle\mathcal{H}_{dd}(t)\rangle_0$ include a constant term, two terms oscillating at the Larmor frequency ω_0, and two terms oscillating at frequency $2\omega_0$. This zero-order result describes the initial response of the spin system in the limit of very high field ($\mathcal{H}_0\gg\mathcal{H}_{dd}$) where spin interactions in pairs predominate. The results are in agreement with the results of Eisenstein's[12] calculations carried to lowest order where coupled spins respond to a step field and oscillate indefinitely. Attenuation effects will appear among an ensemble of spins only after higher order terms are included.

The first-order contribution is

$$\langle\mathcal{H}_{dd}(t)\rangle_1=\mathrm{Tr}\{\mathcal{H}_{dd}^*(-t)\rho_1^*(t)\}=\frac{i}{kT}\int_0^t dt'\,\mathrm{Tr}\{\mathcal{H}_{dd}^*(-t)[\mathcal{H}_{dd}^*(-t'),\mathcal{H}_{dd}]\}, \tag{38}$$

using Eqs. (23) and (28). A direct evaluation of Eq. (38) shows that it contains only odd functions of time and of field. Since $\langle\mathcal{H}_{dd}(t)\rangle$ is an even function of time and of field, the first-order contribution vanishes identically.

A. The Second-Order Contribution

Following the procedure above, the second-order contribution becomes

$$\langle\mathcal{H}_{dd}(t)\rangle_2=-\int_0^t dt'\int_0^{t'}dt''\times\mathrm{Tr}\{\mathcal{H}_{dd}^*(-t)[\mathcal{H}_{dd}^*(-t'),[\mathcal{H}_{dd}^*(-t''),\rho_0]]\}. \tag{39}$$

[12] J. Eisenstein, Phys. Rev. **85**, 603 (1952); J. Jeener, H. Eisendrath, and R. Van Steenwinkel, Phys. Rev. **133**, A478 (1964).

Manipulation of Eq. (39) with the use of (30) and (34) gives

$$\langle \mathcal{H}_{dd}(t)\rangle_2 = -\frac{1}{kT}\sum_{M=-2}^{2}\sum_{M'=-2}^{2}\mathrm{Tr}\{[G_M,\mathcal{H}_{dd}^*(-t)][\mathcal{H}_{dd},G_{M'}]\}\times F(M,M';t), \quad (40)$$

and

$$F(M,M';t)=-\int_0^t\int_0^{t'} dt''dt' \exp(iM\omega_0 t'')\exp(iM'\omega_0 t').$$

The individual traces in the sum of Eq. (40) may be expressed in the general form

$$\mathrm{Tr}\{[G_M,G_{M'}][G_{M''},G_{M'''}]\}.$$

In order that such a trace should not vanish identically, the indices must satisfy the equation $M+M'+M''+M'''=0$. This requirement, together with general properties of the trace leads to the result that Eq. (40) reduces to nine independent trace terms, given in Appendix A. Separate terms from Eq. (40) can be identified with the same time dependence which group together as follows:

$$\langle \mathcal{H}_{dd}(t)\rangle_2=\frac{-1}{kT}\Big[\Gamma_1 t^2\cos\omega_0 t+\Gamma_2 t^2\cos^2\omega_0 t+\frac{\Gamma_3(\omega_0 t)\sin\omega_0 t}{\omega_0^2}+\Gamma_4\frac{(\omega_0 t)\sin 2\omega_0 t}{\omega_0^2}+\Gamma_5\left(\frac{\cos\omega_0 t-1}{\omega_0^2}\right)+\Gamma_6\left(\frac{\cos 2\omega_0 t-1}{\omega_0^2}\right)+\Gamma_7\left(\frac{\cos 3\omega_0 t-1}{\omega_0^2}\right)\Big]. \quad (41)$$

The Γ coefficients are defined in Appendix A in terms of combinations of the traces obtained from Eq. (40). Explicit expressions for the traces are also given in the Appendix, where they are related to H_L^2 and lattice sums for the CaF_2 system. Those readers who are concerned with detailed calculations in problems involving the use of the particular commutators discussed in the Appendix may find them useful and time saving.

Each of the terms in Eq. (41) has an amplitude behavior proportional to t^2 for very small t, and all leading terms in t^2, plus constant terms, are independent of the field H_s. The terms involving Γ_1 and Γ_2 are negative, which indicates that damping of the oscillations must occur in the high-field limit $H_s \gg H_L$. These terms are, in fact, the leading terms in the power series expansion of the rigorous damping function which would be evaluated if our calculations were to be extended to arbitrary high order.

B. Gaussian Damping Function Approximation

In the absence of knowledge of higher order contributions to $\langle \mathcal{H}_{dd}(t)\rangle$ beyond the second order, and because $\langle \mathcal{H}_{dd}(t)\rangle_0+\langle \mathcal{H}_{dd}(t)\rangle_2$ is an even function in t, one can usually approximate the observed damping behavior of the observed $\langle \mathcal{H}_{dd}(t)\rangle$, or $\langle M_z(t)\rangle$, by a Gaussian damping function. Such a function should describe rather well the damping behavior for the few oscillations which occur near $t=0$. Adding Eqs. (37) and (41) gives

$$\begin{aligned}-kT\langle \mathcal{H}_{dd}(t)\rangle_{0,2} &= (\langle \mathcal{H}_{dd}(t)\rangle_0+\langle \mathcal{H}_{dd}(t)\rangle_2)(-kT)\\ &=[1+(H_L^2/H_s^2)A_0]\,\mathrm{Tr}\{G_0^2\}\\ &+2[(1-B_1\omega_L^2 t^2+A_1 H_L^2/H_s^2)\\ &\times\cos\omega_0 t-C_1(H_L^2/H_s^2)\omega_0 t\sin\omega_0 t]\,\mathrm{Tr}\{G_1G_{-1}\}\\ &+2[(1-B_2\omega_L^2 t^2+A_2 H_L^2/H_s^2)\\ &\times\cos 2\omega_0 t-2C_2(H_L^2/H_s^2)\omega_0 t\sin 2\omega_0 t]\,\mathrm{Tr}\{G_2G_{-2}\}\\ &+(\Gamma_7/\omega_0^2)[\cos(3\omega_0 t)-1], \quad (42)\end{aligned}$$

where

$$A_0=-\frac{\Gamma_5+\Gamma_6}{\omega_L^2\,\mathrm{Tr}\{G_0^2\}},$$

$$A_{1,2}=\frac{\Gamma_{5,6}}{2\omega_L^2\,\mathrm{Tr}\{G_{1,2}G_{-1,-2}\}},$$

$$B_{1,2}=-\frac{\Gamma_{1,2}}{2\omega_L^2\,\mathrm{Tr}\{G_{1,2}G_{-1,-2}\}},$$

$$C_1=-\frac{\Gamma_3}{2\omega_L^2\,\mathrm{Tr}\{G_1G_{-1}\}},$$

$$C_2=-\frac{\Gamma_4}{4\omega_L^2\,\mathrm{Tr}\{G_2G_{-2}\}},$$

and

$$\omega_L^2=\gamma^2H_L^2.$$

The second and third square bracket terms in Eq. (42) are of particular interest because they pertain to oscillations observed at Larmor frequencies ω_0 and $2\omega_0$, respectively. At $t=0$, note that $\langle \mathcal{H}_{dd}(t)\rangle_{0,2}=\langle \mathcal{H}_{dd}(i)\rangle$, which indicates, according to Eq. (22), that $\langle M_z(0)\rangle=0$. The last term is indicative of the presence of a component at $3\omega_0$, but proves to be negligible in amplitude compared to the lower frequency terms. The problem now is how to best estimate the damping function. It would not be reasonable to assign an over-all second moment to the Fourier transform of the transient function $\langle \mathcal{H}_{dd}(t)\rangle_{0,2}$ because this estimate would ignore the fact that the resonance lines at frequencies $\sim\omega_0$ and $2\omega_0$ are observed to have different widths and amplitudes.[5] Therefore, by way of example, we may approximate the expression in the second square brackets as

$$Q(\omega_0)=\{(1+A_1H_L^2/H_s^2)\cos[\omega_0 t(1+C_1H_L^2/H_s^2)]\}\times\exp(-B_1\omega_L^2t^2). \quad (43)$$

With the experimental condition that

$$x=C_1(H_L^2/H_s^2)\omega_0 t<1,\quad y=2C_2(H_L^2/H_s^2)\omega_0 t<1,$$
$$\sin(x,y)\approx x,y,\quad \cos(x,y)\approx 1,$$

expanding Eq. (43) gives terms in the second square brackets of Eq. (42); namely,

$$Q(\omega_0)\approx\cos\omega_0 t-C_1(H_L^2/H_s^2)\omega_0 t\sin\omega_0 t+(A_1H_L^2/H_s^2-B_1\omega_L^2t^2)\cos\omega_0 t+O(H_L^4/H_s^4)+O(H_L^2\omega_L^2t^2/H_0^2),$$

if the higher order terms are dropped. The construction given by $Q(\omega_0)$ to describe the oscillations at frequency ω_0 and the damping is justified primarily by the experimental results. Cheng[13] has calculated zero and second moments for lines at both ω_0 and $2\omega_0$ for powder samples of the cubic lattice type. Applying the above reasoning as well to the terms pertaining to $2\omega_0$, the final theoretical expression which approximates the observed transient is given by

$$\begin{aligned}\langle\mathcal{H}_{dd}(t)\rangle_{0,2}&\approx-(1/kT)[(1+A_0H_L^2/H_s^2)\,\mathrm{Tr}\{G_0^2\}\\&+2(1+A_1H_L^2/H_0^2)\cos[\omega_0 t(1+C_1H_L^2/H_s^2)]\\&\times\exp(-B_1\omega_L^2t)\,\mathrm{Tr}\{G_1G_{-1}\}+2(1+A_2H_L^2/H_0^2)\\&\times\cos[2\omega_0 t(1+C_2H_L^2/H_s^2)]\\&\times\exp(-B_2\omega_L^2t^2)\,\mathrm{Tr}\{G_2G_{-2}\}].\end{aligned}\quad(44)$$

The Gaussian damping factor B_2 in Eq. (44) is greater than B_1, so that the oscillation amplitude component at frequency $2\omega_0$ decays more rapidly than the component at ω_0. This behavior agrees with Cheng's[13] result that the second moment of the absorption line at $2\omega_0$ is greater than the second moment at ω_0. The immediate change in the dipole-dipole energy is reflected by those terms proportional to $\mathrm{Tr}\{G_1G_{-1}\}$ and $\mathrm{Tr}\{G_2G_{-2}\}$. These terms can be labeled as nonsecular, which contribute to rapid oscillations of energy between the Zeeman and dipole-dipole reservoirs. The energy proportional to $\mathrm{Tr}\{G_0^2\}$ is constant in Eq. (44), but actually diminishes in time much more slowly than the observed transient decay of the oscillations. This term pertains to the secular energy in the dipole-dipole reservoir, and decays with a time constant given approximately by Caspers[9] as

$$\tau(H_s)\approx\tau(0)\exp(H_s^2/2\langle\Delta H^2\rangle),$$

valid for $H_s\gg H_L$, where $\tau(0)$ is the time constant at $H_s=0$ and $\langle\Delta H^2\rangle$ is a characteristic mean-square local field.

A better approximation to the measured values of $\langle\mathcal{H}_{dd}(t)\rangle$ would of course be possible if the complete fourth-order term $\langle\mathcal{H}_{dd}(t)\rangle_4$ were to be patiently worked out. The third-order term $\langle\mathcal{H}_{dd}(t)\rangle_3$ is zero for the same reasons which make $\langle\mathcal{H}_{dd}(t)\rangle_1=0$. The fourth-order correction would require the computation of 61 traces of the form

$$\mathrm{Tr}\{[G_\alpha,[G_\beta,G_\gamma]][[G_\delta,G_\epsilon],G_\zeta]\}.$$

These would contribute terms at frequencies $4\omega_0$ and $5\omega_0$, and would also entail corrections to the second-order frequencies and amplitudes.

TABLE I. Table of parameters for second-order transient response described by Eq. (44).[a]

Parameter	Powder	⟨100⟩	⟨110⟩	⟨111⟩
$\langle\langle G_0\rangle\rangle$	1/5	0.3975	0.1506	0.0683
$\langle\langle G_1\rangle\rangle$	2/5	0.1367	0.4658	0.5775
$\langle\langle G_2\rangle\rangle$	2/5	0.4658	0.3835	0.3561
A_0	−2/5	−1.395	1.375	12.22
A_1	31/30	3.342	0.456	−0.506
A_2	−5/6	0.209	−1.094	−1.528
B_1	7/30	0.4637	0.1813	0.0789
B_2	1/3	0.9062	0.2398	0.1139
C_1	4/5	0.438	0.885	1.04
C_2	1/15	−0.361	0.174	0.351

[a] See Appendix B for explicit expressions of the parameters.

[13] Hung Cheng, Phys. Rev. **124**, 1359 (1961).

IV. EXPERIMENTAL RESULTS

A. Equilibrium Magnetization Measurements

The theoretical plot of Eq. (21a) for three values of the parameter H_B/H_L is given in Fig. 2 by the smooth curves for H_S along the ⟨111⟩ direction in CaF_2. Also shown are the experimental observations (dark points) of incremental magnetization versus step field for H_S with H_B of approximately 70 G applied at $t_B=200$ μsec. The three theoretical curves are normalized to unity and the experimental plot has been scaled to make its maximum amplitude also unity. Step field H_S is expressed in units of gauss on the top scale and in units of H_L on the bottom scale.

Within the experimental error the maximum incremental magnetization occurs when the step field H_S equals the theoretical local field H_L of 3.25 G. There is good agreement between the experimental results and the theory for $H_B=20H_L\approx70$ G when one considers that the finite rise time of H_B probably reduces the effective value of H_B.

B. Transient Oscillations

Table I lists the numerical values of parameters which enter into Eq. (44), described for each crystal orientation of CaF_2. The experimental results are expressed in terms of the energy ratio obtained from Eq. (22):

$$F(t)=-\frac{H_S\langle\Delta M_z(t)\rangle}{\langle\mathcal{H}_{dd}(i)\rangle}=1-\frac{\langle\mathcal{H}_{dd}(t)\rangle_{0,2}}{\langle\mathcal{H}_{dd}(i)\rangle},\quad(45)$$

where $\langle\mathcal{H}_{dd}(t)\rangle_{0,2}$ is given by Eq. (44). The expression for $F(t)$ can be written as

$$F(t)=\bar{A}_0+\sum_{i=1}^{2}\bar{A}_i\exp(-\bar{B}_i^2t^2)\cos\bar{C}_it,\quad(46)$$

TABLE II. Parameters for theoretical plots of $F(t)$, Eq. (46), given in Figs. 4–9 inclusive.

Figure	CaF_2 Sample	H_S/H_L	$\bar{A}_0$	$\bar{A}_1$	$100\,\bar{B}_1$	$\bar{C}_1$	$\bar{A}_2$	$100\,\bar{B}_2$	$\bar{C}_2$
4	⟨100⟩	7.0	0.6137	−0.1459	5.655	0.5903	−0.4678	7.906	1.162
5	⟨110⟩	7.1	0.8455	−0.4700	3.536	0.6000	−0.3752	4.067	1.183
6	⟨111⟩	7.2	0.9158	−0.5700	2.345	0.6134	−0.3458	2.803	1.211
7	⟨100⟩	3.5	0.6484	−0.1746	5.655	0.2991	−0.4739	7.906	0.5601
8	⟨110⟩	3.5	0.8322	−0.4834	3.536	0.3105	−0.3489	4.067	0.5861
9	⟨111⟩	3.8	0.8725	−0.5549	2.345	0.3351	−0.3176	2.803	0.6397

where

$$\bar{A}_0=1-(1+A_0H_L^2/H_s^2)\,\mathrm{Tr}\{G_0^2\}/\mathrm{Tr}\{\mathcal{H}_{dd}^2\},$$

and

$$\bar{A}_i=-2(1+A_{1,2}H_L^2/H_s^2)\frac{\mathrm{Tr}\{G_{1,2}G_{-1,-2}\}}{\mathrm{Tr}\{\mathcal{H}_{dd}^2\}}.$$

Table II lists the parameters for the theoretical plots of $F(t)$, given in Figs. 4 to 9. Measurements of the transient response were made at step fields $H_s\approx 1.8H_L$, $3.6H_L$, and $7.1H_L$, applied along the ⟨100⟩, ⟨110⟩, and ⟨111⟩ crystal directions. The vertical scales for the experimental curves have been adjusted to fit the first maximum of the theoretical $F(t)$ function given by Eq. (46) in Figs. 4–9. Three scales are given for the time $t(t_B)$: in microseconds; in reciprocal units of the local field angular frequency $\omega_L=\gamma H_L$; and in units of the fluorine (F^{19}) Larmor period $T=2\pi(\gamma_F H)^{-1}$.

For increasing values of $H_s(H_s>H_L)$ the signal-to-noise ratio deteriorates as the magnitude of ΔM_z correspondingly decreases. On the other hand, the theory is expected to give a better description of the results as the ratio H_s/H_L is increased. Best agreement between theory and experiment is found for those measurements made at $H_s\approx 3.6H_L$. Figures 4, 5, and 6 show the main features of the transient response of the magnetization to large step fields. The response consists of damped oscillations with ⟨100⟩ CaF_2 showing the greatest damping and ⟨111⟩ CaF_2 the least. The relative minima that appear near the peak of the first cycle provide evidence for a component oscillating at twice the Larmor frequency. The ratio of second harmonic to fundamental component is greatest for ⟨100⟩ CaF_2 and least for ⟨111⟩ CaF_2. In these figures, the agreement between theory and experiment is rather good up to a time $t_B\sim 2/\omega_L$, and fair thereafter. In Figs. 5 and 6 the experimental curves show greater damping for the third and later full cycles than the theoretical curve, owing probably to the assumption of Gaussian damping functions.

In Figs. 7, 8, and 9 the relative maxima in the first Larmor period are of unequal height. This asymmetry arises because the frequency of the second harmonic component is somewhat less than twice the frequency

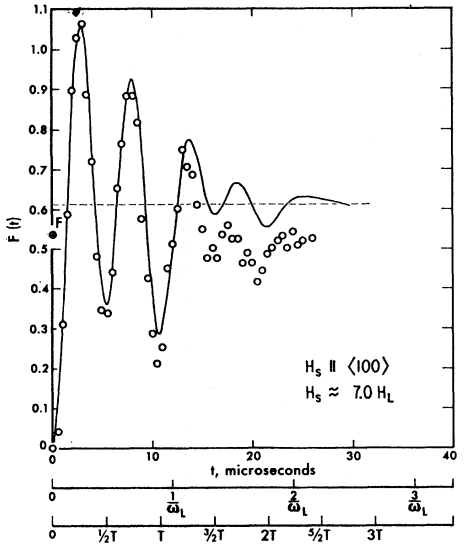

FIG. 4. Transient response of fluorine magnetization in CaF_2 following application of step magnetic fields H_s for various values of H_s and single-crystal orientations of CaF_2 ($H_s\approx 7.0\,H_L$ and parallel to ⟨100⟩ direction).

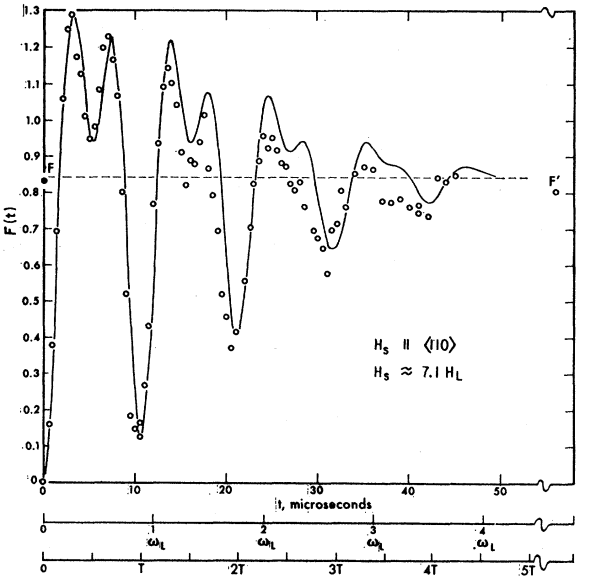

FIG. 5. Transient F magnetization response for $H_s\approx 7.1\,H_L$ parallel to ⟨110⟩ direction.

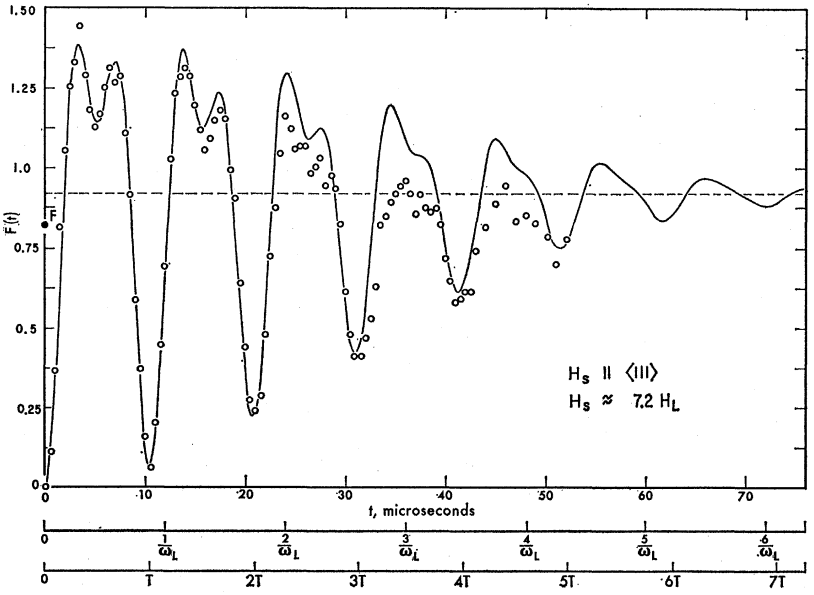

FIG. 6. Transient F magnetization response for $H_s \approx 7.2\, H_L$ parallel to ⟨111⟩ direction.

of the fundamental component. To be sure, damping produces a similar effect, but damping alone is not enough to make the effect as large as it is. For example, if the signs of the frequency shifts for ⟨111⟩ CaF_2 are reversed while keeping the damping unchanged, the asymmetry is reversed.

The dashed horizontal line in each of Figs. 4–9 is the asymptote of the theory which changes in amplitude as a function of H_s, according to the correction terms of the theory. The solid black dots marked F and F' are fiducial point measurements of the magnetization at time $t_B \sim 200$ μsec, where F and F' correspond to the beginning and end of a complete experimental run. For Figs. 7 to 9 the points F and F' are within 3% of the theoretical asymptote.

In Fig. 10 we have plotted the experimental results for low step fields comparable to $1.8H_L$ for all three crystals. At this low field, the theory is in poor agreement with the experimental results, and the theoretical plot has therefore not been included. A smooth curve has been drawn through the points for each orientation of the field. The data have been normalized so that the equilibrium magnetization at $t_B \sim 200$ μsec observed at the start of the run (the point labeled F) is unity. The greatest oscillatory structure and least damping is exhibited by the data taken on ⟨111⟩ CaF_2, just as it appears at the higher fields H_s. Evidence for an absolute frequency shift is given by the pronounced minimum

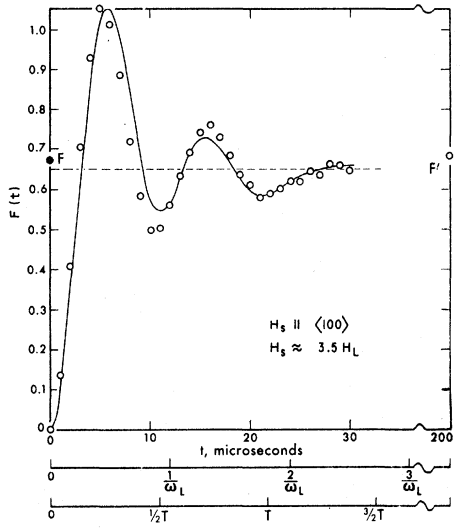

FIG. 7. Transient F magnetization response for $H_s \approx 3.5\, H_L$ parallel to ⟨100⟩ direction.

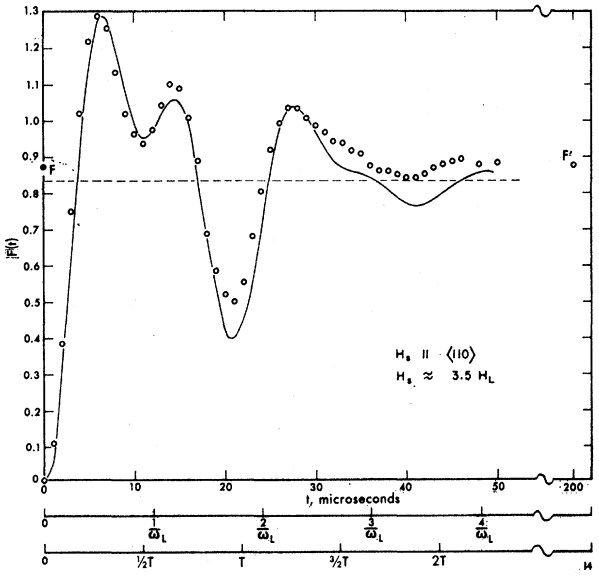

FIG. 8. Transient F magnetization response for $H_s \approx 3.5\, H_L$ parallel to ⟨110⟩ direction.

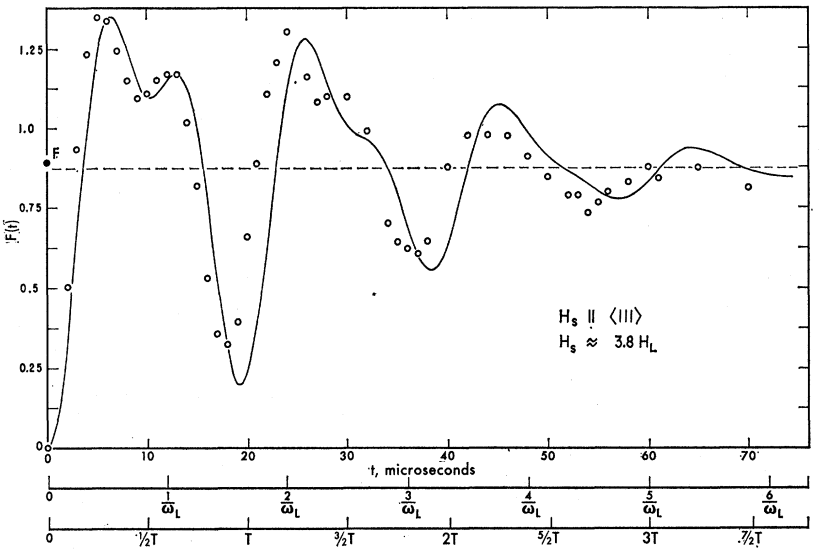

FIG. 9. Transient F magnetization response for $H_s \approx 3.8\,H_L$ parallel to ⟨111⟩ direction.

at about $3T/4$ and a second shallower minimum at about $3T/2$, where T is the period of the nominal Larmor frequency in the field. The subsidiary structure between the maximum at $T/4$ and the minimum at $3T/4$ indicates the presence of a second oscillating component having a frequency less than twice that of the fundamental component.

The data for ⟨100⟩ CaF_2 display the least structure and greatest damping as the strong damping and relatively large second harmonic content combine to produce the minimum near $T/2$. The curve for ⟨110⟩ CaF_2 has intermediate characteristics. The curves for ⟨111⟩ CaF_2 are representative of samples with little secular energy while those for ⟨100⟩ CaF_2 are more representative of samples with a relatively large proportion of secular energy. Presumably powder samples would give experimental plots which look very much like the curves plotted for ⟨110⟩ CaF_2.

The general technique for adiabatic demagnetization and subsequent measurement of nuclear induction signals in high field have been described elsewhere.[14] Particularly unique in the study here is the production of step fields in very short times. A condenser bank is charged to a high voltage and then discharged by a

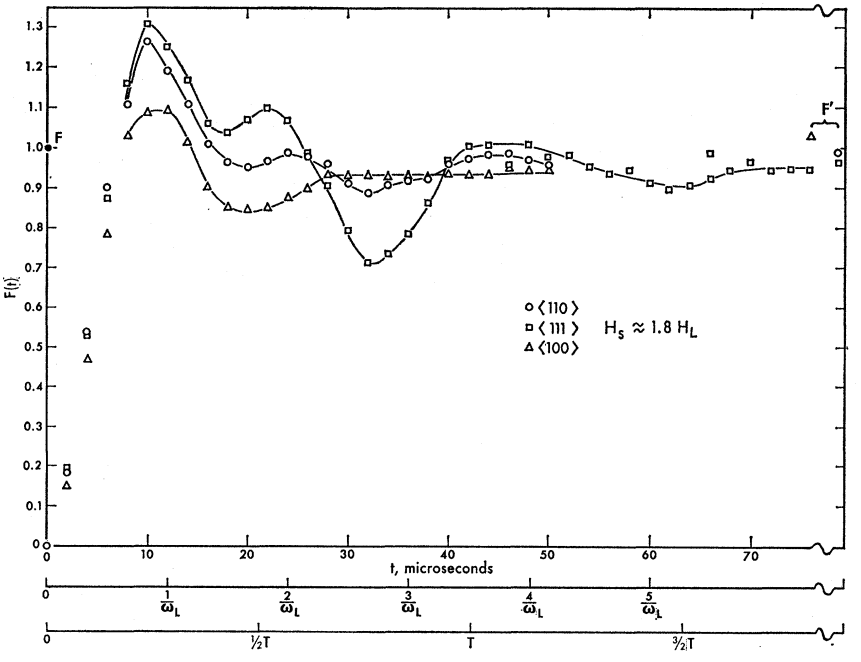

FIG. 10. Transient F magnetization response for $H_s \approx 1.8\,H_L$ parallel to ⟨110⟩, ⟨111⟩, and ⟨100⟩ directions.

[14] W. E. Blumberg, Phys. Rev. **119**, 1842 (1960); P. S. Pershan, Ref. 7.

hydrogen thyratron into a series circuit which includes the step field inductive coil L and a limiting resistor R. The particular circuit used in our application included two thyratrons separated by a large resistance. To produce the first step field H_s, the circuit is closed through the large resistance by one thyratron. At a predetermined time t_B later, the second thyratron is fired, shunting the large resistance and thereby producing the second larger step field H_B.

The L/R of the closed circuit determines the step field rise time if it is not so short as to be affected by the firing time of the thyratron. Since only one coil is used and the charging voltage is usually constant, it follows that H_B has the longest L/R rise time. Normally, the step field $H_B \approx 80$ G turns on in about 3.5×10^{-7} sec, during which time the component of F^{19} magnetization oscillating at $2\omega_0$ could at most precess through an angle of $\pi/4$ rad. This finite rise time is probably the explanation for the failure of the equilibrium magnetization of Fig. 2 to match the theoretical curve for $H_B=20H_L$.

V. CONCLUSIONS

The time dependence of the magnetization of F^{19} nuclei in CaF_2, following the sudden application of a magnetic field, agrees reasonably well with a theory which computes the oscillations in dipole-dipole energy. The observed damping is roughly approximated by a Gaussian-type decay function. Although the damping is not predicted very well for large times, which a fourth-order correction would help to remedy, the decay for short times is in general agreement with linewidth observations in steady-state experiments. In large step fields, the spin system attains internal equilibrium in two stages. In the first stage, which is treated as rigorously as is feasible in this paper, the magnetic oscillations decay in a time $t\sim1/\gamma H_L$. The first and second harmonic Larmor frequencies are displayed, and each frequency component shows amplitude and frequency corrections. The second stage of relaxation is not treated here, where the secular spin-spin energy comes into thermal equilibrium with the Zeeman energy. The theory of Caspers[9] for the latter case is only valid in the limit that $H_s/H_L\gg1$, in which case the experiment is difficult to carry out because the signals are very weak. Very rough measurements indicate that Caspers' theory is not well confirmed in detail although the lack of agreement could be ascribed to the fact that the ratio H_s/H_L did not obey Caspers' condition. Obviously this lack of agreement points out the need for a theory of relaxation of the secular spin energy for the case $H_s\sim H_L$. The theory of the transient response for $H_s \lesssim H_L$ is not discussed, but can be done phenomenologically,[15] using the results of Wright[16] and Broer.[17]

The response of a spin system to a step field not only will take place in the laboratory frame, but occurs as well in experiments which study the behavior of spin order in the rotating frame.[6] The possibilities for facile manipulation of radio-frequency fields H_1 in the rotating frame, with H_1 playing the role of H_s, would require in many respects the same theoretical techniques described in this paper in order to account for transient changes of nuclear magnetization in the rotating frame.

ACKNOWLEDGMENTS

We wish to acknowledge many stimulating and helpful discussions with Dr. A. G. Anderson, Dr. S. R. Hartmann, and Dr. M. Weger. We are indebted to G. W. Leppelmeier for programming the machine calculation of the theoretical curves. One of us (RLS) gratefully acknowledges the support of an NSF Fellowship during the course of this research.

APPENDIX A

There are nine nonvanishing traces of the form $\mathrm{Tr}\{[G_M,G_{M'}][G_{M''},G_{M'''}]\}$, where the G_M are spherical tensor components of the dipole-dipole Hamiltonian. The number is limited to nine because of two restrictions. The number of essentially different commutators $[G_M,G_M]$ is six, while $M+M'+M''+M'''=0$ is the condition for a nonvanishing trace.

The traces of the above form have been calculated for any general number, kind, or distribution of spins. The results of the calculation are given below, where $D=J(J+1)$.

$$K_3=\frac{\mathrm{Tr}\{[G_2,G_{+1}][G_{-1},G_{-2}]\}}{\mathrm{Tr}1}=\tfrac{3}{8}\sum_{k\neq l\neq m} D_kD_lD_m(\gamma_k{}^2\gamma_l\gamma_m)^2(r_{kl}r_{km})^{-6}(1-\zeta_{kl}{}^2)^2(1-\zeta_{km}{}^2)\zeta_{km}{}^2$$
$$+\tfrac{3}{8}\sum_{k\neq l\neq m}{}^{*}\,(D_kD_lD_m)(\gamma_k{}^2\gamma_l\gamma_m)^2(r_{kl}r_{km})^{-6}(1-\zeta_{kl}{}^2)(1-\zeta_{km}{}^2)\zeta_{km}\zeta_{kl}(\xi_{kl}\xi_{km}+\eta_{kl}\eta_{km})$$
$$+\tfrac{3}{8}\sum_{k\neq l\neq m}(D_kD_lD_m)(\gamma_k{}^2\gamma_l\gamma_m)^2(r_{kl}{}^2r_{km}r_{lm})^{-3}\{(1-\zeta_{kl}{}^2)^2\zeta_{km}\zeta_{lm}(\xi_{km}\xi_{lm}+\eta_{km}\eta_{lm})$$
$$+2(1-\zeta_{kl}{}^2)\zeta_{kl}\zeta_{km}[(\xi_{lm}{}^2-\eta_{lm}{}^2)(\xi_{kl}\xi_{km}-\eta_{kl}\eta_{km})+2\xi_{lm}\eta_{lm}(\xi_{kl}\eta_{km}+\eta_{kl}\xi_{km})]$$
$$+(1-\zeta_{kl}{}^2)\zeta_{kl}{}^2[(\xi_{km}{}^2-\eta_{km}{}^2)(\xi_{lm}{}^2-\eta_{lm}{}^2)+4\xi_{km}\eta_{km}\xi_{lm}\eta_{lm}]\}$$
$$+\frac{3}{80}\sum_{k\neq l}D_kD_l(12D_l-9)(\gamma_k\gamma_l)^4(r_{kl})^{-12}(1-\zeta_{kl}{}^2)^3\zeta_{kl}{}^2.$$

[15] R. L. Strombotne, thesis, University of California, 1962 (unpublished).
[16] A. Wright, Phys. Rev. **76**, 1826 (1949).
[17] L. H. Broer, Physica **10**, 801 (1943).

$$K_2=\frac{\mathrm{Tr}\{[G_2,G_0][G_0,G_{-2}]\}}{\mathrm{Tr}1}=\frac{5}{48}\sum_{k\neq l\neq m}(D_kD_lD_m)(\gamma_k{}^2\gamma_l\gamma_m)^2(r_{kl}r_{km})^{-6}(1-\zeta_{km}{}^2)^2(3\zeta_{kl}{}^2-1)^2$$

$$+\frac{1}{48}\sum_{k\neq l\neq m}{}^{*}(D_kD_lD_m)(\gamma_k{}^2\gamma_l\gamma_m)^2(r_{kl}r_{km})^{-6}(3\zeta_{kl}{}^2-1)(3\zeta_{km}{}^2-1)[(\xi_{kl}{}^2-\eta_{kl}{}^2)(\xi_{km}{}^2-\eta_{km}{}^2)+4\xi_{kl}\eta_{kl}\xi_{km}\eta_{km}]$$

$$+\frac{1}{12}\sum_{k\neq l\neq m}(D_kD_lD_m)(\gamma_k{}^2\gamma_l\gamma_m)(r_{kl}{}^2r_{km}r_{lm})^{-3}\{(1-\zeta_{kl}{}^2)^2(3\zeta_{km}{}^2-1)(3\zeta_{lm}{}^2-1)$$

$$+(3\zeta_{kl}{}^2-1)(3\zeta_{lm}{}^2-1)[\xi_{kl}{}^2-\eta_{kl}{}^2)(\xi_{km}{}^2-\eta_{km}{}^2)+4\xi_{kl}\eta_{kl}\xi_{km}\eta_{km}]$$

$$+(3\zeta_{kl}{}^2-1)^2[(\xi_{km}{}^2-\eta_{km}{}^2)(\xi_{lm}{}^2-\eta_{lm}{}^2)+4\xi_{km}\eta_{km}\xi_{lm}\eta_{lm}]\}$$

$$+\frac{1}{160}\sum_{k\neq l}D_kD_l(12D_l+21)(\gamma_k\gamma_l)^4(r_{kl})^{-12}(3\zeta_{kl}{}^2-1)^2(1-\zeta_{kl}{}^2)^2.$$

$$K_1(3)=\frac{\mathrm{Tr}\{[G_2,G_{-1}][G_{-1},G_0]\}}{\mathrm{Tr}1}$$

$$=\tfrac{1}{8}\sum_{k\neq l\neq m}D_kD_lD_m(\gamma_k{}^2\gamma_l\gamma_m)^2(r_{kl}r_{km})^{-6}(3\zeta_{kl}{}^2-1)\zeta_{km}{}^2\sin^2\theta_{km}\sin^2\theta_{kl}\exp[2i(\varphi_{km}-\varphi_{kl})]$$

$$-\tfrac{1}{8}\sum_{k\neq l\neq m}{}^{*}D_kD_lD_m(\gamma_k{}^2\gamma_l\gamma_m)^2(r_{kl}r_{km})^{-6}(1-\zeta_{kl}{}^2)\zeta_{kl}\zeta_{km}(3\zeta_{km}{}^2-1)\sin\theta_{km}\sin\theta_{kl}\exp[i(\varphi_{km}-\varphi_{kl})]$$

$$+\tfrac{1}{8}\sum_{k\neq l\neq m}D_kD_lD_m(\gamma_k{}^2\gamma_l\gamma_m)^2(r_{kl}{}^2r_{km}r_{lm})^{-3}\{2\zeta_{kl}{}^2(3\zeta_{lm}{}^2-1)\sin^2\theta_{kl}\sin^2\theta_{km}\exp[2i(\varphi_{kl}-\varphi_{km})]$$

$$+2\zeta_{lm}\zeta_{km}(3\zeta_{kl}{}^2-1)\sin^2\theta_{kl}\sin\theta_{km}\sin\theta_{lm}\exp[i(\varphi_{km}+\varphi_{lm}-2\varphi_{kl})]$$

$$+\zeta_{km}\zeta_{kl}(3\zeta_{lm}{}^2-1)(1-\zeta_{kl}{}^2)\sin\theta_{kl}\sin\theta_{km}\exp[i(\varphi_{kl}-\varphi_{km})]\}$$

$$-\frac{9}{160}\sum_{k\neq l}D_kD_l(4D_l-3)(\gamma_k\gamma_l)^4(r_{kl})^{-12}\zeta_{kl}{}^2(3\zeta_{kl}{}^2-1)(1-\zeta_{kl}{}^2)^2.$$

$$\zeta_{kl}=\cos\theta_{kl},\quad \xi_{kl}=\sin\theta_{kl}\cos\varphi_{kl},\quad \eta_{kl}=\sin\theta_{kl}\sin\varphi_{kl}.$$

$$K_1(2)=\frac{\mathrm{Tr}\{[G_2,G_{-1}][G_{+1},G_{-2}]\}}{\mathrm{Tr}1}=\tfrac{3}{4}\sum_{k\neq l\neq m}(D_kD_lD_m)(\gamma_k{}^2\gamma_l\gamma_m)^2(r_{kl}r_{km})^{-6}(1-\zeta_{kl}{}^2)^2\zeta_{km}{}^2(1-\zeta_{km}{}^2)$$

$$+\tfrac{3}{8}\sum_{k\neq l\neq m}(D_kD_lD_m)(\gamma_k{}^2\gamma_l\gamma_m)^2(r_{kl}{}^2r_{km}r_{lm})^{-3}\{(1-\zeta_{kl}{}^2)\zeta_{km}\zeta_{lm}(\xi_{km}\xi_{lm}+\eta_{km}\eta_{lm})$$

$$+\zeta_{kl}{}^2(1-\zeta_{kl}{}^2)[(\xi_{km}{}^2-\eta_{km}{}^2)(\xi_{lm}{}^2-\eta_{lm}{}^2)+4\xi_{km}\eta_{km}\xi_{lm}\eta_{lm}]\}$$

$$+\frac{9}{80}\sum_{k\neq l}D_kD_l\left(6D_l+\frac{11}{2}\right)(\gamma_k\gamma_l)^4(r_{kl})^{-12}\zeta_{kl}{}^2(1-\zeta_{kl}{}^2)^3.$$

$$K_1(1)=\frac{\mathrm{Tr}\{[G_1,G_0][G_0,G_{-1}]\}}{\mathrm{Tr}1}=\frac{7}{24}\sum_{k\neq l\neq m}(D_kD_lD_m)(\gamma_k{}^2\gamma_l\gamma_m)^2(r_{kl}r_{km})^{-6}\zeta_{kl}{}^2(1-\zeta_{kl}{}^2)(3\zeta_{km}{}^2-1)^2$$

$$+\frac{5}{24}\sum_{k\neq l\neq m}{}^{*}(D_kD_lD_m)(\gamma_k{}^2\gamma_l\gamma_m)^2(r_{kl}r_{km})^{-6}(3\zeta_{kl}{}^2-1)(3\zeta_{km}{}^2-1)\zeta_{kl}\zeta_{km}(\xi_{kl}\xi_{km}+\eta_{kl}\eta_{lm})$$

$$+\tfrac{1}{12}\sum_{k\neq l\neq m}(D_kD_lD_m)(\gamma_k{}^2\gamma_l\gamma_m)(r_{kl}{}^2r_{km}r_{lm})^{-3}[\zeta_{kl}{}^2(1-\zeta_{kl}{}^2)(3\zeta_{km}{}^2-1)(3\zeta_{lm}{}^2-1)$$

$$+(3\zeta_{kl}{}^2-1)(3\zeta_{km}{}^2-1)\zeta_{kl}\zeta_{lm}(\xi_{kl}\xi_{lm}+\eta_{kl}\eta_{lm})+(3\zeta_{kl}{}^2-1)^2\zeta_{km}\zeta_{lm}(\xi_{km}\xi_{lm}+\eta_{km}\eta_{lm})]$$

$$+\frac{1}{160}\sum_{k\neq l}D_kD_l(84D_l-5)(\gamma_k\gamma_l)^4(r_{kl})^{-12}(3\zeta_{kl}{}^2-1)\zeta_{kl}{}^2(1-\zeta_{kl}{}^2).$$

$$K_0(3)=\frac{\mathrm{Tr}\{[G_{+2},G_{-2}][G_{-1},G_{+1}]\}}{\mathrm{Tr}1}=\tfrac{3}{8}\sum_{k\neq l\neq m} D_kD_lD_m(\gamma_k{}^2\gamma_l\gamma_m)^2(r_{kl}{}^2r_{km}r_{lm})^{-3}(1-\zeta_{kl}{}^2)\zeta_{kl}\zeta_{km}$$
$$\times[(\xi_{lm}{}^2-\eta_{lm}{}^2)(\xi_{kl}\xi_{km}-\eta_{kl}\eta_{km})+2\xi_{lm}\eta_{lm}(\xi_{kl}\eta_{km}+\eta_{kl}\xi_{km})]$$
$$-\frac{9}{80}\sum_{k\neq l} D_kD_l(2D_l+1)(\gamma_k\gamma_l)^4(r_{kl})^{-12}(1-\zeta_{kl}{}^2)^3\zeta_{kl}{}^2.$$

$$K_0(2)=\frac{\mathrm{Tr}\{[G_2,G_{-2}][G_2,G_{-2}]\}}{\mathrm{Tr}1}=\tfrac{3}{16}\sum_{k\neq l\neq m} D_kD_lD_m(\gamma_k{}^2\gamma_l\gamma_m)^2(r_{kl}r_{km})^{-6}(1-\zeta_{kl}{}^2)^2(1-\zeta_{km}{}^2)^2$$
$$+\frac{9}{320}\sum_{k\neq l} D_kD_l(8D_l-1)(\gamma_k\gamma_l)^4(r_{kl})^{-12}(1-\zeta_{kl}{}^2)^4.$$

$$K_0(1)=\frac{\mathrm{Tr}\{[G_{+1},G_{-1}][G_{+1},G_{-1}]\}}{\mathrm{Tr}1}=\frac{9}{4}\sum_{k\neq l\neq m} D_kD_lD_m(\gamma_k{}^2\gamma_l\gamma_m)^2(r_{kl}r_{km})^{-6}\zeta_{kl}{}^2(1-\zeta_{kl}{}^2)\zeta_{km}{}^2(1-\zeta_{km}{}^2)$$
$$+\tfrac{3}{4}\sum_{k\neq l\neq m}{}^{*} D_kD_lD_m(\gamma_k{}^2\gamma_l\gamma_m)^2(r_{kl}r_{km})^{-6}\zeta_{kl}{}^2\zeta_{km}{}^2[(\xi_{kl}{}^2-\eta_{kl}{}^2)(\xi_{km}{}^2-\eta_{km}{}^2)+4\xi_{kl}\eta_{kl}\xi_{km}\eta_{km}]$$
$$+\tfrac{3}{4}\sum_{k\neq l\neq m} D_kD_lD_m(\gamma_k{}^2\gamma_l\gamma_m)^2(r_{kl}{}^2r_{km}r_{lm})^{-3}$$
$$\times\{4\zeta_{kl}{}^2\zeta_{km}\zeta_{lm}[(\xi_{kl}{}^2-\eta_{kl}{}^2)(\xi_{km}\xi_{lm}-\eta_{km}\eta_{lm})+2\xi_{kl}\eta_{kl}(\xi_{km}\xi_{lm}+\eta_{km}\eta_{lm})]+\zeta_{kl}{}^2(1-\zeta_{kl}{}^2)\zeta_{km}\zeta_{lm}(\xi_{km}\xi_{lm}+\eta_{km}\eta_{lm})\}$$
$$+\frac{9}{4}\sum_{k\neq l} D_kD_l(D_l+1)(\gamma_k\gamma_l)^4(r_{kl})^{-12}\zeta_{kl}{}^4(1-\zeta_{kl}{}^2)^2.$$

The notation $\sum^*$ means that the sum is very nearly a vanishing sum in the following sense: The sum over three indices $k\neq l\neq m$ may be transformed into a sum over two indices, say $k\neq l$, that is multiplied by the total number of spins N. The sum over two indices, in turn, may be expressed in terms of unrestricted sums by use of the relation of the form

$$\sum_{k\neq l}\mathfrak{A}_k\mathfrak{B}_l=\sum_k\mathfrak{A}_k\cdot\sum_l\mathfrak{B}_l-\sum_k\mathfrak{A}_k\mathfrak{B}_k.$$

When this process has been used on the sum $\sum^*$ the sum over a single index is a sum over terms in $1/r^{12}$ and normally contributes only one or two percent to the total trace. The product of two sums vanishes identically for a cubic lattice that has the z axis parallel to a $\langle 100\rangle$, $\langle 110\rangle$, or $\langle 111\rangle$ direction and is probably completely negligible for other orientations and other lattices, though there is a possibility that for particular orientations in particular lattices it may contribute significantly to the trace.

Two of the traces given above have been calculated by other investigators who have also included the exchange Hamiltonian with G_0. Cheng[13] has calculated $K_1(1)$ and K_2 for a system of like spins and evaluated them for powder samples of simple cubic and body-centered cubic lattices. Caspers[9] has calculated $K_1(1)$ for electronic spins. His result is in essential agreement with the result given above, although it seems he has assumed that the sum labeled as $\sum^*$ vanishes identically. Caspers evaluated $K_1(1)$ for a simple cubic lattice with the z axis parallel to a $\langle 100\rangle$ direction and also for a face-centered cubic lattice with the z axis parallel to a $\langle 100\rangle$ direction and with it parallel to a $\langle 111\rangle$ direction.

The dominant sums of the various traces give reasonably good approximate values for the traces when only one type of spin is present. The dominant sums are those sums with $(r_{kl})^{-6}(r_{km})^{-6}$ and which are not starred. The trace $K_0(3)$ has no such sum. The trace $K_1(3)$ is the only complex trace. It is not expected to be a significant trace in comparison with the others because of its complicated orientation dependence.

The Γ coefficients of Eq. (41) are defined:

$$\Gamma_1=-K_1(1),$$
$$\Gamma_2=-K_2,$$
$$\Gamma_3=K_3-2K_0(1)-K_1(2),$$
$$\Gamma_4=2K_3+2K_2-2K_1(2)-K_0(2),$$
$$\Gamma_5=-\frac{5}{2}K_3+\frac{10}{3}K_1(2)+6K_1(1)+\frac{16}{3}K_0(3)-4K_0(1),$$
$$\Gamma_6=2K_3+\frac{3}{2}K_2-\frac{10}{3}K_1(2)-\frac{4}{3}K_0(3)-K_0(2),$$
$$\Gamma_7=\tfrac{1}{2}K_3.$$

APPENDIX B

From evaluation of the traces the following general approximate expressions for spin systems with one type

of spin are obtained:

$$K_3 \approx -\frac{1}{2} WS_1S_2/S^2,$$

$$K_2 \approx -\frac{5}{3} WS_0S_2/S^2,$$

$$K_1(1) \approx -\frac{7}{6} WS_1S_0/S^2,$$

$$K_1(2) \approx WS_1S_2/S^2,$$

$$K_1(3) \approx 0,$$

$$K_0(1) \approx -\frac{3}{4} W(S_1/S)^2,$$

$$K_0(2) \approx W(S_2/S)^2,$$

$$K_0(3) \approx 0,$$

where

$$W = \tfrac{1}{3}\gamma^4 H_L^4 ND,$$
$$H_L^2 = \gamma^2 D \sum r^{-6} = \gamma^2 DS/4,$$

N is the total number of spins, and $S = S_0 + S_1 + S_2 = 4\sum r^{-6}$. The lattice sums S_i are

$$S_0 = \sum_k r_k^{-6}(3\cos^2\theta_k - 1)^2,$$
$$S_1 = 12 \sum_k r_k^{-6} \sin^2\theta_k \cos^2\theta_k,$$
$$S_2 = 3 \sum_k r_k^{-6} \sin^4\theta_k,$$

where θ_k is the angle between the field direction and the vector from the origin to the lattice site k.

In most instances these approximations are accurate to a few percent. However, when H_s is along the $\langle 100 \rangle$ direction, A_2, B_2, and C_2, and to a lesser extent A_0, will require more exact evaluation because of the poor approximation to K_2 given by one term. In constructing the theoretical curves in the body of the paper great care was taken to properly evaluate the coefficients B_1 and B_2. The approximations given here were used in evaluating the remaining parameters.

In terms of these approximate traces the various coefficients A, B, and C in Eqs. (42), (43), and (44) are given by

$$A_0 = -(A_1S_1 + A_2S_2)/S_0,$$
$$A_1 = (84S_0 - 36S_1 + 25S_2)/(12S),$$
$$A_2 = (15S_0 - 14S_1 - 6S_2)/(6S),$$
$$A_3 = S_1S_2/(4S^2),$$
$$B_1 = 7S_0/(6S),$$
$$B_2 = 5S_0/(3S),$$
$$C_1 = (3S_1 + S_2)/(2S),$$
$$C_2 = -(10S_0 - 3S_1 - 3S_2)/(6S)$$
$$= -(13S_0 - 3S)/(6S).$$

In Table I, numerical values of the above parameters are given together with the parameters:

$$\langle\langle G_0 \rangle\rangle = \mathrm{Tr}\{G_0^2\}/\mathrm{Tr}\{\mathcal{H}_{dd}^2\} = S_0/S,$$
$$\langle\langle G_1 \rangle\rangle = 2\,\mathrm{Tr}\{G_1G_{-1}\}/\mathrm{Tr}\{\mathcal{H}_{dd}^2\} = S_1/S,$$
$$\langle\langle G_2 \rangle\rangle = 2\,\mathrm{Tr}\{G_2G_{-2}\}/\mathrm{Tr}\{\mathcal{H}_{dd}^2\} = S_2/S.$$

The lattice sums S_1, S_2, S_3, accurate to a few percent, were evaluated up to and including a distance of 7 lattice constants. A cutoff error correction was made by integrating over a sphere beyond the 7th lattice constant to a distance out to infinity. Sums over $(r_{kl}^2 r_{km} r_{lm})^{-3}$ were carried out to at least two lattice constants, beyond which major contributions for each $\mathbf{r}_{kl}$ were singled out. The latter sums have errors no greater than 15%, but do not have a major effect on most of the K values, which are generally accurate to a few percent. The only exception is K_2, when H_s is parallel to the $\langle 100 \rangle$ direction.